SPHERIC 2022
INTERNATIONAL WORKSHOP

INGV
OSSERVATORIO ETNEO
SEZIONE DI CATANIA

Università di Catania

E·R·C·O·F·T·A·C

SPHERIC

SPHERIC 2022

CATANIA, ITALY, 6–9 JUNE 2022

Proceedings of the 16th SPHERIC International Workshop

Edited by
Giuseppe Bilotta

SPHERIC 2022

Proceedings of the 16th SPHERIC International Workshop

Catania, Italy, 6–9 June 2022
Istituto Nazionale di Geofisica e Vulcanologia
Università di Catania

Edited by
Giuseppe Bilotta

Published by the Istituto Nazionale di Geofisica e Vulcanologia
ISBN 979-12-8028-205-7

Acknowledgements

The 16th SPHERIC International Workshop is supported by the Osservatorio Etneo of the Istituto Nazionale di Geofisica e Vulcanologia, the Università di Catania and ERCOFTAC.

INGV OSSERVATORIO ETNEO SEZIONE DI CATANIA

Università di Catania

ERCOFTAC

To our colleagues from the Osservatorio Etneo, Monastero dei Benedettini, Museo della Rappresentazione and the Laboratorio di Idraulica go our deepest and sincere thanks for their logistical support. Our gratitude extends to all the members of the SPHERIC Steering Committee, and the chair and vice chair in particular, for their continued guidance in the organization of the workshop. This Workshop would not have been possible without your support.

SPHERIC 2022
INTERNATIONAL WORKSHOP

Cover photo: May 2022 Mt Etna eruption © Francesco Zuccarello.

Foreword

Dear Delegate,

the Osservatorio Etneo, Catania section of the Istituto Nazionale di Geofisica e Vulcanologia, in collaboration with the Università di Catania, is delighted to host the 16th SPHERIC International Workshop.

SPHERIC, the ERCOFTAC Special Interest Group that represents the community of researchers and industrial users of Smoothed Particle Hydrodynamics, has made outstanding efforts to support and foster the development of SPH with online and hybrid events in these difficult times, finding new and creative ways to bring people together and keep the interest for SPH alive inside and outside the community. The choice between a virtual and an on-site event for the 16th edition of the SPHERIC International Workshops has been a difficult one to make. On the one hand, the still problematic international situation would have obstructed participation; on the other, the kind and level of inter-personal exchange that can only be achieved by meeting in-person remains an important aspect of the scientific growth of the community. We have taken a gamble of sorts, and we appreciate the effort of all of you, those that have had the opportunity to come, as well as those that could not make it, in supporting our choice.

In the now well-established tradition of the SPHERIC International Workshops, the programme of this edition offers a Training Day for researchers and users that are starting their work on SPH, and two challenging keynotes. As usual, the Libersky Prize will be awarded for the best contribution from student delegates; the 16th SPHERIC International Workshop also presents for the third time the Joe Monaghan Prize, a recognition to the most important work published on the SPHERIC Grand Challenges between 2013 and 2018.

The contributions that you can find in these Proceedings were selected by our Scientific Committee from over 80 high-level proposed abstracts. They are a testament to the excellent quality of the research being conducted both on the fundamentals of the SPH method and on its application to a wide variety of fields, from engineering to medicine, from geophysics to material sciences.

New and exciting times await Smoothed Particle Hydrodynamics and the SPHERIC community, and it is a great pleasure and honour to share these moments with you.

Come for the science, stay for the food!
Welcome to Catania,

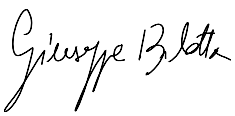

Giuseppe Bilotta
Chair, Local Organizing Committee
16th SPHERIC International Workshop

Scientific Committee

Dr. Alex Crespo (Universidade de Vigo, Ourense, Spain)
Dr. Abbas Khayyer (Kyoto University, Japan)
Dr. David Le Touzé (Ecole Centrale de Nantes, France)
Dr. Nathan Quinlan (National University of Ireland, Galway, Ireland)
Dr. Stefano Sibilla (Università di Pavia, Italy)
Dr. Angelo Tafuni (New Jersey Institute of Technology, US)
Dr. Renato Vacondio (Università di Parma, Italy)
Dr. Antonio Gil (Swansea University, UK)
Dr. Andrea Colagrossi (CNR-INM, Italy)
Dr. Ben Rogers (University of Manchester, UK)
Dr. Salvatore Marrone (CNR-INM, Italy)
Dr. Peter Eberhard (University of Stuttgart, Germany)
Dr. Matthieu De Leffe (Siemens Digital Industries, France)
Dr. Giuseppe Bilotta (Istituto Nazionale di Geofisica e Vulcanologia, Italy)
Dr. Ha Bui (Monash University, Australia)
Dr. Raj Das (RMIT University, Australia)
Dr. Steven Lind (University of Manchester, UK)
Dr. Georgios Fourtakas (University of Manchester, UK)
Dr. Chun Hean Lee (Universiy of Glasgow, UK)
Dr. Moncho Gómez-Gesteira (Universidade de Vigo, Spain)
Dr. Xu Fei (Northwestern Polytechnical University, China)
Dr. Antonio Souto Iglesias (UPM, Spain)
Dr. Rouhollah Fatehi (Persian Gulf University, Iran)
Dr. Xiangyu Hu (Technical University of Munich, Germany)
Dr. Pengnan Sun (Sun Yat-sen University, China)
Dr. Tom De Vuyst (University of Hertfordshire, UK)

Local Organizing Committee

Dr. Giuseppe Bilotta
Dr. Annalisa Cappello
Dr. Gaetana Ganci

Table of contents

Alternative and novel formulations (S4)

Practical and industrial applications I: automotive and aerospace engineering (S5)

Convergence, consistency and stability II (S6)

Energy dissipation evaluation in violent 3D sloshing flows subject to vertical accelerations

Julien Michel, Danilo Durante, Salvatore Marrone
CNR-INM Institute of marine engineering
National Research Council
Rome, Italy,
salvatore.marrone@cnr.it

Andrea Colagrossi
CNR-INM & LHEEA Lab. (UMR CNRS)
National Research Council & Ecole Centrale Nantes
Rome, Italy & Nantes, France

***Abstract*—The present research activity is devoted to the use of fuel sloshing to reduce the design loads on aircraft wings. These are highly flexible structures that can significantly deform under gust loads. Wings house the fuel tanks, and generally carry an amount of fuel comparable in weight to that of their structural components. In the present research the δ-LES-SPH model was adopted to investigate the damping effect of fuel sloshing on the dynamics of flexible wing-like structures. This represents quite a challenging task for SPH and more generally, for CFD tools, as the vertical accelerations involved in the present research can reach 10g. The resulting flow is extremely complex due to the high turbulence developed, the violent impacts and intense fragmentation of the air-liquid interface. In the present work three-dimensional simulations are considered and the 3D effects on the energy dissipation mechanisms. The results are also compared with two-dimensional numerical simulations performed in previous SPHERIC articles, with the aim of comparing the flow evolution, the forces on the tank and the dissipated energy against experimental data.**

I. Introduction

The basic problem of liquid sloshing involves the estimation of the hydrodynamic pressure distribution, forces, moments and natural frequencies of the free surface oscillation. The sloshing motion is characterised by an infinite number of natural frequencies, but only the few lowest modes are the most likely to be excited by the tank motion [12], [16].

From the physical point of view, the study of the dissipation induced by a free-surface flow is arduous, especially in the presence of wave breaking. [24] presented a review of studies dedicated to the dissipation caused by wave breaking.

A recent and attractive example of an industrial sloshing problem, that has increasingly received attention, concerns the kerosene containers placed inside aircraft wings subjected to external wind gusts. Although typical attitude corrections cause weak fuel sloshing motions because of the low accelerations involved,sudden strong gusts accelerate the fuel transversely up to values of 10g, which results in amplitudes comparable to the tank dimensions and frequencies higher than 5 Hz (see [14]). This fluid motion, which several experiments have demonstrated to play a role on the damping of the wing vibrations, is significantly different from typical sloshing flows: the fuel is continuously broken into several jets and drops, whilst violently slamming alternately upward and downward against the tank walls.

Disregarding their industrial impact, very few studies dealing with vertically sloshing flows are found in the literature. Experimentally, one of the first studies dealing with this problem was [7] and, more recently, [13], [30].

From the numerical point of view, violent internal flows are challenging to simulate and mesh-based numerical approaches may suffer from significant mass loss if *ad-hoc* strategies are not adopted. Conversely, particle based approaches such as SPH are more suitable for these kinds of simulations where the free surface is strongly and rapidly deformed in jets and fragmented in sprays and drops.

In [20], the initial stages of such violent flows, where the liquid is mainly driven by inertia because of the strong accelerations, are referred to as "shaken flow". Later stages of the problem, where most of the energy has been dissipated and the tank accelerations become smaller than gravity, are classified as "sloshing flows". In [20], the δ-LES-SPH method was used to study the energy dissipation mechanisms, occurring in shaken flows, for tanks subjected to vertical oscillatory motions with accelerations as high as $10g$. In a second paper by [17] the experiments of [21] were used as reference for comparisons with the numerical simulations.

In the present paper the same experimental campaign of [21] is taken into account and, similarly to [20], the δ-LES-SPH approach is adopted for the simulation of the liquid phase only, neglecting the air phase. Unlike the work of [20] and [17], where the analysis was entirely carried out under the 2D assumption, here the analysis is fully 3D, thus implying additional complications in accurately resolving the flow field, as will be stressed in the following.

One of the typical drawbacks of the standard SPH method is the so-called "tensile instability" which develops inside the fluid domain inducing numerical cavitations in low pressure regions. Conversely, in the δ-LES-SPH model adopted in the present work, a particle shifting technique (PST) enforcing uniform distributions, discussed in [29], is adopted to avoid the development of tensile-instability. Furthermore, the use of PST largely improves the accuracy of the integral interpolations allowing a more accurate evaluation of pressure and vorticity

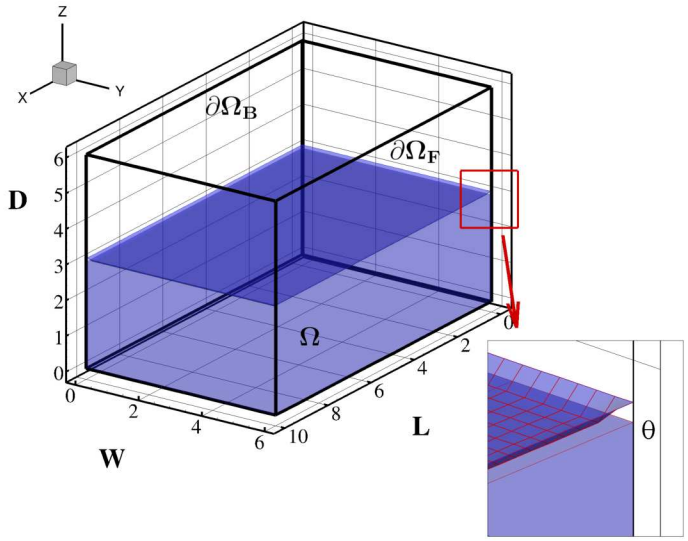

Figure 1. Experimental box sketch with highlight of the filled volume. The axes scales are in cm. Bottom-right: an enlarged view of the liquid meniscus.

fields. Finally, a Large Eddy Simulation (LES) approach based on the classical Smagorinsky model is included in the numerical scheme (see [4], [11] for details) so that the energy contributions coming from unresolved turbulent scales are taken into account.

II. Problem description

In the present numerical study the conditions adopted in the experimental campaign by [21] are applied. In that work a violent sloshing flow in a vertically moving tank was experimentally studied. A tank measuring $10 \times 6 \times 6$ cm is connected to a set of 6 springs, 3 on the upper side and 3 on the lower side, as sketched in figure 2.

In the present work, water and oil are considered as sloshing liquids. The tank is filled up to 50% of its volume (water mass of m_l = 0.18 kg and oil m_l = 0.162 kg). When the springs are released, for both the liquids, the tank oscillates at a characteristic frequency of about f_0 = 6.51 Hz reaching a maximum acceleration $a_{\max}$ of about $8.8g$ and a maximum velocity $U_{\max}$ of about 2.3 m/s. More details on the experiment can be found in the article by [21].

The problem geometry considered in the present work is sketched in figure 1, where L = 10 cm, D = 6 cm, W = 6 cm and H = 3 cm. In the same plot the liquid menisci due to the contact angle between the lateral walls and the liquid surface are depicted and enlarged in the inset. The Reynolds number of the problem is referred to the maximum tank velocity (Re = $U_{max}L/\nu$) where ν is the kinematic viscosity of the fluid.

The tank motions are imposed and are only in the vertical direction. The law of motion is taken from acceleration measurements in [21] and the motion follows a decay law. The resulting Reynolds number at the initial stage is of order 10^5 for water and 10^3 for oil.

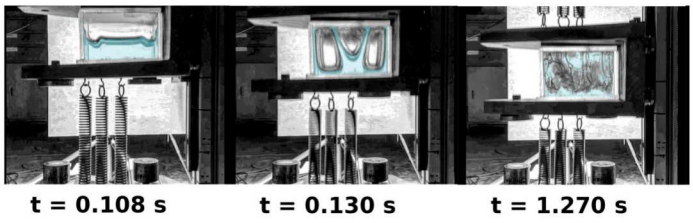

Figure 2. Experimental snapshots of the SDOF vertical sloshing water experiments carried out in [21] for 50% filling level.

III. Governing equations

In the present work a three-dimensional fluid domain Ω is considered with its boundaries which are composed by the tank walls $\partial\Omega_B$ and the free surface $\partial\Omega_F$. The flow evolution is governed by the Navier-Stokes equations (see also [17], [20]):

$$\begin{cases} \dfrac{D\rho}{Dt} = -\rho\,\mathrm{div}(\boldsymbol{u}), & \dfrac{D\boldsymbol{u}}{Dt} = \boldsymbol{g} + \dfrac{\mathrm{div}(\mathbb{T})}{\rho} \\ \dfrac{De}{Dt} = \dfrac{\mathbb{T}:\mathbb{D}}{\rho}, & \dfrac{D\boldsymbol{r}}{Dt} = \boldsymbol{u}, \qquad p = f(\rho) \end{cases} \tag{1}$$

where D/Dt represents the Lagrangian derivative, $\boldsymbol{u}$ the flow velocity, $\boldsymbol{r}$ the position of the material points, ρ the fluid density, e the specific internal energy, $\mathbb{T}$ the stress tensor, $\mathbb{D}$ the rate of strain tensor and $\boldsymbol{g}$ the gravitational acceleration.

The thermal conductivity and the surface tension effects are neglected and the liquid is assumed to be Newtonian.

Eq. (1) can be either solved in an Inertial Frame of Reference (I-FoR) where the tank is moving or in a Non-inertial Frame of Reference (Ni-FoR) moving with tank motion. Although the description of the phenomena in both frames of reference does not affect the evaluation of the energy dissipated during the liquid motions, different numerical approaches may lead to different numerical errors, depending on this choice. Due to its easier implementation the Ni-FoR is generally preferred, as it avoids tank motion. It was therefore adopted in the present work.

For the liquid medium, the effects of entropy/temperature on the pressure are assumed to be negligible. Therefore, the pressure p is assumed to depend only on the density. Furthermore, since a weakly-compressible condition is assumed, a simple linear equation of state can be adopted $p = c_0^2\,(\rho - \rho_0)$ where c_0 plays the role of a constant speed of sound of the liquid and ρ_0 is the density at the free-surface (where p is assumed to be equal to zero). In order to avoid too small time steps, c_0 is always set lower than its physical counterpart (in the present work, about two orders of magnitude lower). The weakly-compressible constraint , however, must be checked in order to guarantee the weakly-compressible regime (see [5]).

The use of a single-phase model implies the neglect of the air contained in Ω. This assumption may appear inappropriate for violent sloshing simulations where air entrapment is unavoidable. In [19], it was shown that, although the air phase plays a relevant role in the flow evolution, the evaluation of the

energy dissipation in violent flows even under the single-phase hypothesis is still accurate enough.

As far as surface tension effects are concerned, these are relevant above all during the initial stage. As remarked in [17], [20] during the initial intense vertical acceleration, a Rayleigh–Taylor instability develops. The latter is triggered by the fluid meniscus formed at the intersection between the lateral walls and the liquid surface and numerically modelled as indicated in figure 1. In the evolution just afterwards, the role of the surface tension becomes negligible according to the velocity and length scales considered, as also explained in [8]. Therefore, the surface tension force terms are neglected while initial effect of surface tension is recovered by appropriately setting the initial meniscus free-surface deformation with an angle $\theta = 45°$(see inset of figure 1).

Finally, concerning the use of the artificial speed of sound, as discussed in [18] and in [22], if the weakly-compressible regime is satisfied the energy dissipation linked to the water impacts using equation (1) is consistent with the one predicted by incompressible flow models.

IV. Numerical scheme

In this section the δ-LES-SPH model presented in [4], [23] is briefly recalled. The interested reader is addressed for all the details to the articles cited therein. The governing equations (1) are discretized according to the Smoothed Particle Hydrodynamics numerical approach as follows:

$$\begin{cases} \dfrac{\mathrm{d}\rho_i}{\mathrm{d}t} = \displaystyle\sum_j \left[-\rho_i\ (\boldsymbol{u}_{ji} + \delta\boldsymbol{u}_{ji}) + (\rho_j\ \delta\boldsymbol{u}_j + \rho_i\ \delta\boldsymbol{u}_i)\right] \cdot \boldsymbol{F}_{ij} + \mathcal{D}_i^{\rho} \\ \rho_i \dfrac{\mathrm{d}\boldsymbol{u}_i}{\mathrm{d}t} = \displaystyle\sum_j \left[-(p_j + p_i)\ \mathbb{I} + \rho_0(\boldsymbol{u}_j \otimes \delta\boldsymbol{u}_j + \boldsymbol{u}_i \otimes \delta\boldsymbol{u}_i)\right] \cdot \boldsymbol{F}_{ij} + \\ \qquad\qquad + \boldsymbol{F}_i^v + \rho_i \boldsymbol{g}\,, \qquad \boldsymbol{F}_{ij} := \nabla_i W_{ij} V_j \\ \dfrac{\mathrm{d}\boldsymbol{r}_i}{\mathrm{d}t} = \boldsymbol{u}_i + \delta\boldsymbol{u}_i, \quad V_i(t) = m_i \,/\, \rho_i(t), \quad p = c_0^2(\rho - \rho_0) \end{cases} \tag{2}$$

where the index i refers to the considered particle and j refers to neighbour particles of i. The vector $\boldsymbol{F}_i^v$ is the net viscous force acting on the particle i, while $\delta\boldsymbol{u}$ is the Particle Shifting velocity field which regularizes the spatial distribution of the particles during their motion. The mass m_i of the $i-$th particle is assumed to be constant during its motion. The particles are set initially on a Cartesian lattice with spacing Δr, and hence, the volumes V_i are initially evaluated as Δr^3. The particle masses m_i are calculated through the initial density field (using the equation of state and the initial pressure field) and remain constant during the time evolution. The volumes V_i change in time accordingly with the particle density (see last row of eq. of (2)). The spatial gradients are approximated through the convolution with a kernel function W_{ij}. Following [4], a C2-Wendland kernel is adopted in the present work.

The time derivative d/dt used in (2) indicates a quasi-Lagrangian derivative, since the particles are moving with the modified velocity $(\boldsymbol{u} + \delta\boldsymbol{u})$ and the above equations are written in an Arbitrary Lagrangian-Eulerian framework (see [5]. Because of this, the continuity and the momentum equations contain terms with spatial derivatives of $\delta\boldsymbol{u}$ (for details, the interested reader is referred to [5]).

The notation $\boldsymbol{u}_{ji}$ in (2) indicates the differences $\boldsymbol{u}_j - \boldsymbol{u}_i$ and the same holds for $\delta\boldsymbol{u}_{ji}$ and $\boldsymbol{r}_{ji}$.

The term $\mathcal{D}_i^{\rho}$ is the numerical diffusive term introduced by [1] for the $\delta - SPH$ model to filter out the spurious high-frequency noise in the pressure field. Following [4] this term is rewritten within an LES framework.

The viscous forces $\boldsymbol{F}^v$ are expressed as:

$$\begin{cases} \boldsymbol{F}_i^v := K \displaystyle\sum_j (\mu + \mu_{ij}^T)\, \pi_{ij}\, \nabla_i W_{ij}\, V_j \\ \pi_{ij} := \dfrac{\boldsymbol{u}_{ij} \cdot \boldsymbol{r}_{ij}}{||\boldsymbol{r}_{ji}||^2} \qquad \mu_{ij}^T := 2\, \dfrac{\mu_i^T\, \mu_j^T}{\mu_i^T + \mu_j^T} \end{cases} \tag{3}$$

where $K := 2(n+2)$ being n is the number of spatial dimensions and C_S is the so called Smagorinsky constant set equal to 0.18 (see [28]). The viscous term (3) contains both the effect of the real viscosity μ as well as the one related to the local turbulent viscosity μ_i^T defined as: $\mu_i^T := \rho_0\,(C_S\, l)^2\, ||\mathbb{D}_i||$, where $l = 2.7\Delta r$ is the support of the kernel W for three spatial dimensions ($l = 4\Delta r$ in two dimensions, see [20]) and represents the length scale of the filter adopted for the sub-grid model. The norm $||\mathbb{D}||$ is equal $\sqrt{2\mathbb{D} : \mathbb{D}}$ and the velocity gradient is evaluated through a renormalized interpolation (see *e.g* [2]). Finally, the Particle Shifting velocity law $\delta\boldsymbol{u}$ adopted is given in [20].

A. Boundary conditions

The governing equations (1) are coupled with kinematic and dynamic free-surface boundary conditions on $\partial\Omega_F$, while on the solid surfaces $\partial\Omega_B$ the no-slip boundary condition needs to be enforced. Concerning the former, free-surface boundary conditions are intrinsically satisfied in SPH methods (see [10]). On the other hand, in SPH it is difficult to resolve thin wall boundary layers (WBL) unlike mesh-based methods. Indeed, the use of smaller particles close to the walls implies large CPU costs linked to the explicit time integration of the scheme, as the time steps decrease proportionally to the particle size. Consequently, if the fluid viscosity is significantly low (*i.e.* high Reynolds numbers) very thin WBLs are developed. Because they are too demanding in terms of computational resources to be well resolved, a simple no-penetration boundary condition (free-slip) is preferred. Regarding the simulations with oil, these are performed at a Reynolds number of about 4,660. The same particle size as for water is sufficient to resolve the boundary layer developed by the oil, thus allowing the no-slip conditions to be considered.

V. Considerations on the energy dissipation

Following the analysis performed in [3] and in [23] the energy balance for the particle system can be extended to the δ-LES-SPH equations (2). For the sake of brevity, only the main terms are briefly reported in this section. The δ-LES-SPH energy balance can be written as:

$$\dot{\mathcal{E}}_M + \dot{\mathcal{E}}_C = \mathcal{P}_V + \mathcal{P}_V^{turb} + \mathcal{P}_N + \mathcal{P}_{ext} \qquad \mathcal{P}_N := \mathcal{P}_\delta + \mathcal{P}(\delta\boldsymbol{u}) \tag{4}$$

where $\mathcal{E}_M$ is the mechanical energy of the particle system, formed by kinetic energy $\mathcal{E}_K$ and potential energy $\mathcal{E}_P$. Within the weakly compressible regime, the elastic energy term $\mathcal{E}_C$ is generally negligible in the energy balance; hence it is not considered in the following discussion.

The external power $\mathcal{P}_{ext}$ exerted by the tank walls on the fluid is evaluated through the mutual interaction between fluid and solid particles, as detailed in [3] and in [9]. The power related to the viscous forces contains the quantity $\mathcal{P}_V^{turb}$ which refers to the viscous dissipation of the modelled sub-grid scales, and $\mathcal{P}_V$ refers to the resolved scales. Finally, the term $\mathcal{P}_N$ takes into account the effect of the density diffusion $\mathcal{P}_\delta$ (see [23]) and the term related to the particle shifting $\delta\boldsymbol{u}$, *i.e.* $\mathcal{P}(\delta\boldsymbol{u})$. Both these terms are related to the stability of the scheme and are collected together in $\mathcal{P}_N$ as a numerical diffusion term. Finally, the discrete form of the energy dissipated, $\mathcal{E}_{diss}$, can be expressed as:

$$\mathcal{E}_{diss} = \int_{t_0}^{t} \mathcal{P}_{diss}\ dt, \qquad \mathcal{P}_{diss} := \mathcal{P}_V + \mathcal{P}_V^{turb} + \mathcal{P}_N \quad (5)$$

where t_0 is the initial time instant of the simulation.

During the impacts energy losses occur, therefore the weakly-compressible approach acts in such a way that acoustic waves, coming from the conversion of mechanical energy and travelling at velocity c_0 are formed and then dissipated through the density diffusion term, *i.e.* $\mathcal{P}_\delta$, as investigated in [23].

When no impacts occur and vortices are generated during post-impact events, the mechanical energy is mainly dissipated by the viscous terms ($\mathcal{P}_V + \mathcal{P}_V^{turb}$) rather than by $\mathcal{P}_\delta$. However, by increasing the spatial resolution both $\mathcal{P}_N$ and $\mathcal{P}_V^{turb}$ decrease, whereas $\mathcal{P}_V$ increases. Indeed, as suggested by [26], for a good LES simulation the resolved turbulent kinetic energy should be greater than the modelled energy. Therefore, the power associated with real viscosity $\mathcal{P}_V$ (which depends upon the resolved velocity gradients) should be greater than $\mathcal{P}_N$ and $\mathcal{P}_V^{turb}$. It is worth noting that even in the discrete form $\mathcal{E}_C$, $\mathcal{P}_V$, $\mathcal{P}_V^{turb}$ and $\mathcal{P}_\delta$ are invariant when switching the reference frame from inertial to non-inertial and vice-versa.

Integrating in time the energy balance (4) between the time instants t_0 and t we obtain:

$$\mathcal{E}_M(t) - \mathcal{E}_M(t_0) = \mathcal{W}_{ext} + \mathcal{E}_{diss}\,, \quad (6)$$

where W_{ext} is the vertical work exerted by the liquid on the tank. By subtracting the inertial term from F_z, the force F_z^{dyn} linked to the deformation of the liquid inside the tank is obtained:

$$F_z^{dyn}(t) := F_z(t) - M_{liquid}\,[-g - a_{tank}(t)] \quad (7)$$

with M_{liquid} the mass of the liquid contained in the tank and a_{tank} the vertical tank acceleration. According to such a decomposition, the energy balance can be rewritten as:

$$\begin{cases} [\mathcal{E}_M(t) - \mathcal{E}_M^{stat}(t)] - [\mathcal{E}_M(t_0) - \mathcal{E}_M^{stat}(t_0)] = \mathcal{W}_{ext}^{dyn} + \mathcal{E}_{diss}\,, \\ \mathcal{W}_{ext}^{dyn} := -\int_{t_0}^{t} F_z^{dyn}(t)\, v_{tank}(t)\ dt\,, \\ \mathcal{E}_M^{stat} := M_{liquid}\left(\frac{1}{2}v_{tank}^2 + g\ z_{tank}\right) \end{cases} \quad (8)$$

where $\mathcal{E}_M^{stat}$ is the mechanical energy of liquid linked to the tank motion only. The term z_{tank} refers to the tank bottom vertical elevation from its initial position, where it is assumed $\mathcal{E}_M(t_0) = \mathcal{E}_M^{stat}(t_0)$. The dynamical work $\mathcal{W}_{ext}^{dyn}$ is the work related to the fluid domain deformation only, *i.e.* due to the sloshing motion. At the final time of the simulation t_f the liquid may be assumed at rest, so that the left-hand side of equation (8) becomes negligible and it follows that:

$$\mathcal{E}_{diss}(t_f) = -\mathcal{W}_{ext}^{dyn}(t_f) \quad (9)$$

From this relation it results that from the measure of the force F_z on the tank and its velocity v_{tank} it is possible to evaluate the experimental dynamical work $\mathcal{W}_{ext}^{dyn}$ and therefore the liquid dissipation $\mathcal{E}_{diss}(t_f)$.

VI. Numerical results

In this section the law of motion resulting from the experiment of [21] is imposed on the tank. The law of motion presents an exponential decay due to the energy that is quickly dissipated by the liquid, and to a lesser extent, by the springs and the supporting rails.

In addition to the study of the energy dissipation under decaying motion, this test case allows for a comparison of the obtained forces (and related work) acting on the tank with those recorded in the experiment. The maximum amplitude of the oscillation motion, taken from recordings in the experiment, is $2A/L = 1.14$. The frequency of motion is defined as $f_0 = \sqrt{k/m}\ /\ 2\pi = 6.51$ Hz, where k is the spring stiffness and m the sum of the masses of the tank, the liquid and the springs. The period $T = 1/f_0 = 0.154$s is assumed as the reference time scale. The reference velocity is $U_{max} = 2\pi A/T = 2.33$ m/s. The corresponding Reynolds number depends on the fluid tested: for the water Re = 233,000, whereas for the oil it is 4,660.

In figure 3 the recorded motion of the tank is plotted in terms of the acceleration of the tank considering both water and oil. When the tank is filled with water the motion is more rapidly damped with respect to the oil case. The maximum acceleration reached during the experiment is close to 10g which is of the same order of magnitude as limit design cases of an airliner wing during a wind gust [15].

The resolution is the same for both cases with $N = 75 = H/\Delta r$ the discretization of the liquid depth at rest, so that the final number of particles is about 2.8 million. The time step used for the simulations is $\Delta t = 7\mu s$, implying that the total iterations at the end of the simulation are about $570,000$. This large number is the main reason for the challenging

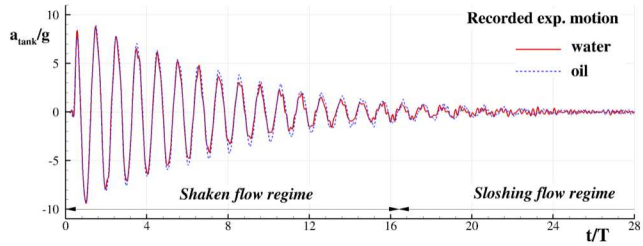

Figure 3. Tank acceleration recorded in the experiment of [21]: tank with water (solid line) tank with oil (dashed line).

computational cost of these simulations although the number of particles may not appear to be so large (see also [25]).

A. *Flow field comparisons*

In this section the results obtained from 3D simulations for both oil and water cases are discussed. The same results are also compared to the outcomes of the 2D simulations from [17]. In figures 4 and 6 the vortex structures of oil simulations are depicted along with the vorticity fields obtained from 2D simulations at the same simulation time. The 3D vortex structures are identified through the Q-criterion. Specifically, iso-surfaces with Q=50 are depicted. For the sake of clarity the 3D free-surface is made transparent. A rendering of the free surface for the first two time instants is provided at the bottom of figure 4. In figures 5 and 7 the same is reported for the water test case.

The 3D flow evolves similarly to the 2D one discussed in [17]: in the initial stage, during the first upward acceleration of the tank, a small free-surface wave is generated due to the collapse of the menisci at the lateral walls. The waves travel from the lateral walls towards the centre of the tank. When the tank inverts its acceleration direction for the first time, a Rayleigh-Taylor instability is triggered. The inception of this instability starts from the small gravity waves generated by the menisci collapse. The fluid viscosity plays a significant role in the intensity of this first impact.

As shown in figure 4, for the oil case in 2D (top-right plot) two main thin jets moving towards the tank ceiling are discernible close to the lateral walls; similarly, in 3D (top-left and bottom-left plot) a thin film of fluid moves, parallel to the lateral walls, towards the tank ceiling. The water case, shown in figure 5, is clearly more energetic as a large part of the fluid in the middle of the tank moves upward. In 2D the rising fluid is essentially distributed onto the main diverging jets, with several other smaller jets ejected at the same time. In 3D the moving liquid forms four main jets corresponding to the four tank corners. The small structures observed in 2D are not visible in this case as the resolution is significantly coarser ($N = 400$ versus $N = 75$).

When the fluid impacts the ceiling (middle plots and bottom-right plot of figures 4 and 5), the different flow dynamics explained above induce different types of impacts: in the oil case when the jets impact the ceiling the rectangular

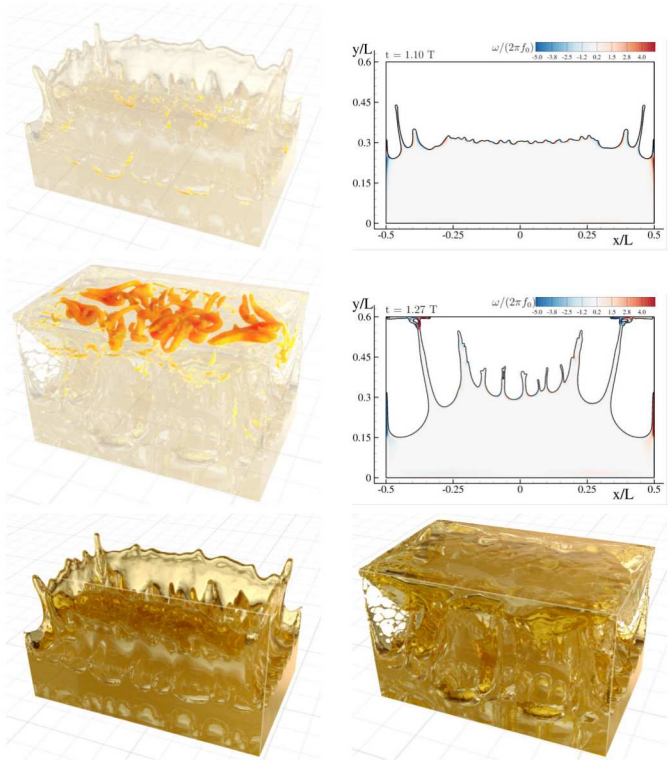

Figure 4. Top, middle: comparisons between 3D (**left**) and 2D (**right**) simulations of oil sloshing. In 3D the iso-Q surfaces for $Q = 50$ are plotted against the vorticity in 2D. Bottom: rendering of the free surface at the same time instants.

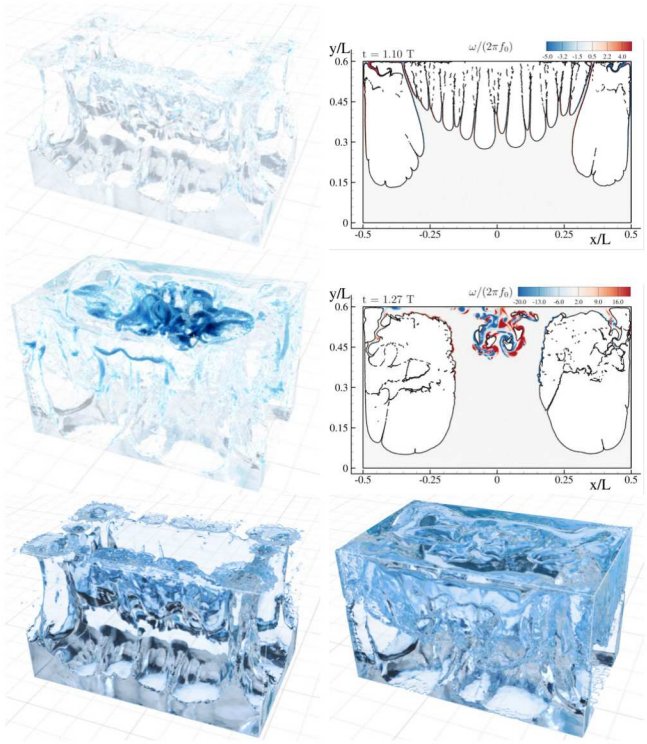

Figure 5. Top, middle: comparisons between 3D (**left**) and 2D (**right**) simulations of water sloshing. In 3D the iso-Q surfaces for $Q = 50$ are plotted against the vorticity in 2D. Bottom: rendering of the free surface at the same time instants.

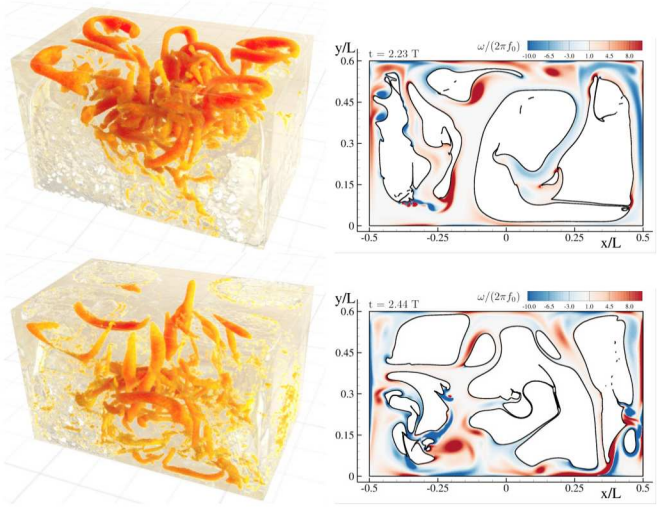

Figure 6. Comparisons between 3D (**left**) and 2D (**right**) simulations of oil sloshing. In 3D the iso-Q surfaces for $Q = 50$ are plotted against the vorticity in 2D. The corresponding times of 2D simulations are reported at the top left of the corresponding frame.

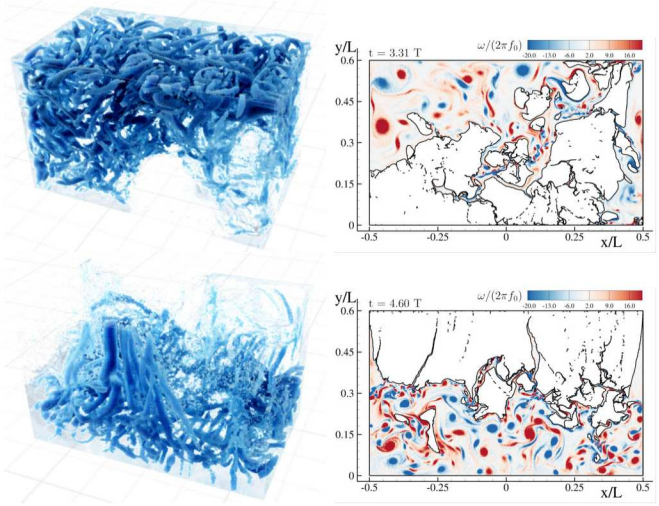

Figure 7. Comparisons between 3D (**left**) and 2D (**right**) simulations of water sloshing. In 3D the iso-Q surfaces for $Q = 50$ are plotted against the vorticity in 2D. The corresponding times of 2D simulations are reported at the top left of the corresponding frame.

film expands over the ceiling and produces large and tangled vortex tubes occupying a large region of the tank wall; in the water case a larger amount of liquid impacts slightly in advance with respect to the oil case. This generates a pocket at the centre of the tank ceiling enclosing the vortex structures generated by the previous impingement of the liquid jets. The 2D evolution for water is quite similar to its 3D counterpart, whereas for the oil the impact is not complete at the same simulation time and only the impinging of the two initial jets occurs (see middle right plot of figure 4).

After the first impact, the fluid starts a series of cyclical impacts against the ceiling and the floor of the tank. As shown in figure 6 and 7, in 2D the fluid is mostly fragmented in multiple jets and the energy is dissipated in free-surface reconnections and the consequent generation of vorticity. Lower viscosity is associated to thinner jets and a larger number of vortices, as visible in the water vorticity fields shown in the right column of figure 7. Conversely, the oil case is characterised by thicker jets and the liquid covers almost the entire solid surface.

In the 3D simulations a proliferation of vortex tubes during the impacts is observed. This is particularly evident for the water case (left column of figure 7) in which highly entangled vortex structurs are spread all over the liquid domain at the impact instant. On the other hand, higher viscosity levels correspond to a smaller number of vortex tubes, mostly characterised by larger diameter size (left column of figure 6).

When the transition from the "shaken" flow regime to the "sloshing flow" regime occurs, as explained in [17], the flow is still highly fragmented with vorticity distributed on a wide range of length scales. Afterwards, the fluid regains its initial compact shape with gravity waves travelling over the liquid surface and impacting against the lateral walls and, occasionally, the tank ceiling.

B. Discussion of the energy dissipation

In this section the dissipated energy predicted by the numerical solver is analysed and compared to experimental data. In figure 8 the dissipated energy, $\mathcal{E}_{diss}$ (see eq. (5)), computed by SPH is plotted against the non-dimensional time for four different spatial resolutions varying from $N = 22$ to $N = 75$. A 1.5 ratio between two successive discretization levels was adopted. In the same figure the evaluation of the dynamical work done by solid walls in the experiments at the final time, $-\mathcal{W}_{ext}^{dyn}(t_f)$ (see eq. (8)), is also reported. As stressed in section V, the dynamical work is related to the fluid dissipated energy by relation (9) where it is highlighted that $\mathcal{E}_{diss}$ and $-\mathcal{W}_{ext}^{dyn}$ are expected to be very close at the final stage of the simulation when the fluid is almost at rest. The dissipated energy is made non-dimensional by the potential energy $\Delta\mathcal{E} = \rho_W g\ LWH\ 2A = 0.201$ J for water and 0.181 J for oil.

In the left plot of figure 8 the convergence analysis of $\mathcal{E}_{diss}$ is shown for the oil test case. No significant variations are observed for the different resolutions: this suggests that even the lowest discretisation, $N = 22$, is sufficient to resolve the inertial range of the turbulent cascade. The final value of $\mathcal{E}_{diss}$ is quite close to the experimental evaluation of $-\mathcal{W}_{ext}^{dyn}$.

For the water case, right plot of figure 8, the situation is significantly different: convergence of the dissipated energy is not attained for the considered resolutions. Even if the experimental value is close to the result at $N = 75$, it is expected that a further increase in the resolution will result in a larger value of the final dissipated energy. This aspect is further discussed later in the section.

Considering the oil case for the higher resolution the ratio between the turbulent and the fluid viscosity μ_T/μ is lower

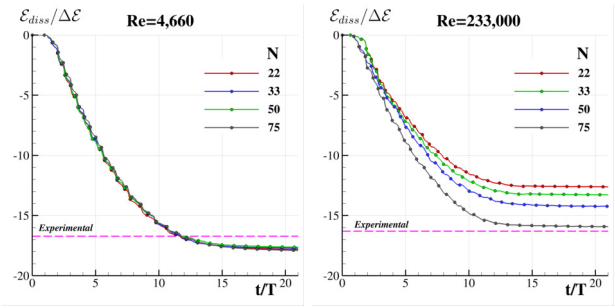

Figure 8. Convergence of the dissipated energy for oil (**left**) and water (**right**). With the dashed line, the experimental data obtained for $-\mathcal{W}_{ext}^{dyn}$ at final time, as shown in figure 9.

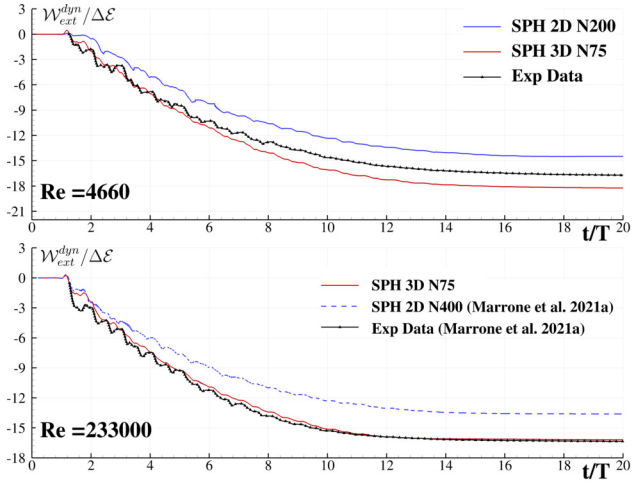

Figure 9. Time histories of the dynamical work compared with experiments and 2D simulations for oil (**top** plot) and water (**bottom** plot).

than 0.5 almost everywhere, thus indicating that the sub grid scales are well modelled and that the inertial range is correctly captured. For the coarser case the ratio does not exceed 5.0, which is still a good value for a well resolved LES simulation [27]. Conversely, the turbulent viscosity largely exceeds the fluid one for the water case even at the highest resolution $N = 75$, the observed values are around $\mu_T/\mu \approx 30$, whereas for a good LES the ratio should be of order $O(1)$ [27]. For coarser resolution the sub-grid scales are, *a fortiori*, not adequately modelled and the cut-off of the energy exchange takes place within the inertial range [6]. These aspects provide further elements for the discussion of the convergence analysis in figure 8: it can be easily concluded that for the water test case the highest resolution is still too coarse to obtain a convergent result. Regarding this topic, in [17] an in-depth study was performed in the 2D framework.

Although in 2D the effect of the vorticity is more intense and a direct comparison with 3D is not possible, in the former work it was observed that a convergent result was obtained at Re=233,000 with a spatial resolution as high as $N = 400$. In that case the observed maximum ratio was $\mu_T/\mu = 5$. Such a resolution in 3D corresponds to about 430 million of particles and 425 days of computing time on 1000 cluster cores (the computational cost is about $150\mu s$ per iteration and per particle).

For the water case the 2D and 3D results are rather similar, although the resolutions for the two approaches are significantly different (*i.e.* $N = 400$ versus $N = 75$). Conversely, for the oil case the force predicted in 2D underestimated the 3D force, and this is mainly linked to effects of the boundary layer region on whole walls of the 3D box. For both water and oil the force peaks are better resolved in the 3D solution with respect to its 2D counterpart in which they are rather smoothed. The predicted forces in 3D are, generally, in good agreement with the experimental data and follow quite closely the damped oscillations of the vertical force on the box.

In figure 9 the time histories of the dynamical work $-\mathcal{W}_{ext}^{dyn}$ defined in (8) are reported for both fluids. In the top plot of figure 9 the dynamical work for the oil is shown together with the experimental data by [21] and a 2D simulation at $N = 200$. The comparison shows a fair agreement between the numerical solution and the experiments. The 3D solution after an initial overlapping with the experimental data, at around $t/T = 6$ slightly diverges and overestimates the dynamical work. On the other hand, the 2D solution underestimates the dynamical work during the entire time evolution. The final gap between the numerical outcomes and the experimental value is about 9% and 13% respectively for the 3D and the 2D solutions. As far as the water simulations are concerned, the dynamical work is reported in the bottom plot of figure 9. In this case too, the 3D solution is in better agreement with the experimental data than the 2D solution. However, it is important to recall that the resolution adopted for the water is not sufficient and, most likely, a further increase in the numerical resolution could lead to a different final value of the dissipated energy.

It is worth noting that the final value of $\mathcal{W}_{ext}^{dyn}$ observed in the 3D solutions is very close to the final value of $\mathcal{E}_{diss}$ for both water and oil cases. This is expected from eq. (9) but it is not a trivial result from a numerical point of view, as the two quantities are computed in very different ways: $\mathcal{E}_{diss}$ is measured during the simulation by means of eq. (5) while $\mathcal{W}_{ext}^{dyn}$ is computed *a posteriori* through eq. (8).

Summarising, the 3D simulations tend to overestimate the energy dissipation and this is probably linked to the role of the air phase which is neglected in the present work. In this regard, further investigations are needed. However, taking into account the air phase with an SPH model leads to a considerable increase in the CPU costs linked to the doubling of the total number of particles and to a further reduction in the time step. On the other hand, in order to obtain a more reliable validation procedure, further improvements are also needed from the experimental side. It is important to underline, indeed, that the experimental estimation of $\mathcal{W}_{ext}^{dyn}$ is challenging since even small time delays of a few milliseconds between the force and the tank velocity measurements may induce significant errors in the evaluation of the external work. Therefore, a sensitivity analysis targeting this specific quantity is needed in order to

measure the uncertainty which affects the reference data.

VII. Conclusions

In the present paper, the work of [17] was extended to the 3D framework. Challenging numerical simulations of the violent sloshing flow in a moving tank were performed with specific focus on the prediction of the mechanical energy dissipated by the fluid during the motion. Two different Reynolds numbers, corresponding to oil and water, were considered and the numerical outcomes were compared to existing experimental data. The δ-LES-SPH approach was adopted and its capabilities in simulating these kinds of flows were discussed. Three-dimensional features of the flow were observed and compared to previous 2D studies. With a maximum resolution of $N = 75$ particles on the liquid depth, we found that the simulations converge well for the lower Reynolds number case in terms of sub-grid scales modelling and dissipated energy, whereas some issues persist with the water case due to the limited spatial discretization. With respect to the highly resolved 2D simulations performed in [17], the final results are closer to the experiments in terms of forces acting on the tank and time history of the work done by solid walls.

Acknowledgements

The work was supported by the SLOWD project which received funding from the European Union's Horizon 2020 research and innovation programme under grant agreement No 815044.

The SPH simulations performed under the present research project were obtained with the SPH-Flow solver, a software developed within a collaborative consortium composed of Ecole Centrale Nantes, NextFlow Software company and CNR-INM.

The authors acknowledge Paolo Colagrossi, CEO of Punkt.ink company, for the post processing and the rendering of 3D SPH data.

References

[1] M. Antuono, A. Colagrossi, and S. Marrone. Numerical diffusive terms in weakly-compressible SPH schemes. *Computer Physics Communications*, 183(12):2570–2580, 2012.

[2] M. Antuono, A. Colagrossi, S. Marrone, and D. Molteni. Free-surface flows solved by means of SPH schemes with numerical diffusive terms. *Computer Physics Communications*, 181(3):532–549, 2010.

[3] M. Antuono, S. Marrone, A. Colagrossi, and B. Bouscasse. Energy balance in the δ-SPH scheme. *Computer Methods in Applied Mechanics and Engineering*, 289:209–226, 2015.

[4] M. Antuono, S. Marrone, A. Di Mascio, and A. Colagrossi. Smoothed Particle Hydrodynamics method from a large eddy simulation perspective. Generalization to a quasi-lagrangian model. *Physics of Fluids*, 33(1):015102, 2021.

[5] M. Antuono, P.N. Sun, S. Marrone, and A. Colagrossi. The δ-ALE-SPH model: An arbitrary lagrangian-eulerian framework for the δ-SPH model with particle shifting technique. *Computers & Fluids*, 216:104806, 2021.

[6] A. Aprovitola and F.M. Denaro. On the application of congruent upwind discretizations for large eddy simulations. *Journal of Computational Physics*, 194(1):329–343, 2004.

[7] H. Bredmose, M. Brocchini, D.H. Peregrine, and L. Thais. Experimental investigation and numerical modelling of steep forced water waves. *Journal of Fluid Mechanics*, 490:217–249, 2003.

[8] J. Calderon-Sanchez, J. Martinez-Carrascal, L.M. Gonzalez-Gutierrez, and A. Colagrossi. A global analysis of a coupled violent vertical sloshing problem using an sph methodology. *Engineering Applications of Computational Fluid Mechanics*, 15(1):865–888, 2021.

[9] J.L. Cercos-Pita, M. Antuono, A. Colagrossi, and A. Souto-Iglesias. SPH energy conservation for fluid–solid interactions. *Computer Methods in Applied Mechanics and Engineering*, 317:771–791, 2017.

[10] A. Colagrossi, M. Antuono, and D. Le Touzé. Theoretical considerations on the free-surface role in the Smoothed-particle-hydrodynamics model. *Physical Review E*, 79(5), 2009.

[11] A. Di Mascio, M. Antuono, A. Colagrossi, and S. Marrone. Smoothed particle hydrodynamics method from a large eddy simulation perspective. *Physics of Fluids*, 29(3):035102, 2017.

[12] O.M. Faltinsen and A.N. Timokha. *Sloshing*, volume 577. Cambridge university press Cambridge, 2009.

[13] F. Gambioli and A. Malan. Fuel loads in large civil airplanes. In *Proc. 4th Spheric Workshop, Nantes, France*, volume 247, 2009.

[14] F. Gambioli and A. Malan. Fuel loads in large civil airplanes. In *International Forum on Aeroelasticity and Structural Dynamics IFASD 2017*, 2017.

[15] F. Gambioli, R. Alegre Usach, J. Kirby, T. Wilson, and P. Behruzi. Experimental evaluation of fuel sloshing effects on wing dynamics. In *International Forum on Aeroelasticity and Structural Dynamics. Savannah, Georgia, USA, paper*, volume 139, 2019.

[16] R.A. Ibrahim. *Liquid sloshing dynamics: theory and applications*. Cambridge University Press, 2005.

[17] S. Marrone, A. Colagrossi, J. Calderon-Sanchez, and J. Martinez-Carrascal. Numerical study on the dissipation mechanisms in sloshing flows induced by violent and high-frequency accelerations. II. comparison against experimental data. *Phys. Rev. Fluids*, 6:114802, Nov 2021.

[18] S. Marrone, A. Colagrossi, A. Di Mascio, and D. Le Touzé. Prediction of energy losses in water impacts using incompressible and weakly compressible models. *Journal of Fluids and Structures*, 54:802–822, 2015.

[19] S. Marrone, A. Colagrossi, A. Di Mascio, and D. Le Touzé. Analysis of free-surface flows through energy considerations: Single-phase versus two-phase modeling. *Physical Review E*, 93(5):053113, 2016.

[20] S. Marrone, A. Colagrossi, F. Gambioli, and L. González-Gutiérrez. Numerical study on the dissipation mechanisms in sloshing flows induced by violent and high-frequency accelerations. I. theoretical formulation and numerical investigation. *Phys. Rev. Fluids*, 6:114801, Nov 2021.

[21] J. Martinez-Carrascal and L.M. González-Gutiérrez. Experimental study of the liquid damping effects on a sdof vertical sloshing tank. *Journal of Fluids and Structures*, 100:103172, 2021.

[22] D.D. Meringolo, A. Colagrossi, S. Marrone, and F. Aristodemo. On the filtering of acoustic components in weakly-compressible SPH simulations. *Journal of Fluids and Structures*, 70:1–23, 2017.

[23] D.D. Meringolo, S. Marrone, A. Colagrossi, and Y. Liu. A dynamic δ-sph model: How to get rid of diffusive parameter tuning. *Computers & Fluids*, 179:334–355, 2019.

[24] M. Perlin, W. Choi, and Z. Tian. Breaking waves in deep and intermediate waters. *Annual review of fluid mechanics*, 45:115–145, 2013.

[25] C. Pilloton, A. Bardazzi, A. Colagrossi, and S. Marrone. SPH method for long-time simulations of sloshing flows in lng tanks. *European Journal of Mechanics - B/Fluids*, accepted on, 2022.

[26] Stephen B Pope. *Turbulent flows*. IOP Publishing, 2001.

[27] P. Sagaut. *Large eddy simulation for incompressible flows: an introduction*. Springer Science & Business Media, 2006.

[28] J. Smagorinsky. General circulation experiments with the primitive equations: I. the basic experiment. *Monthly weather review*, 91(3):99–164, 1963.

[29] P.N. Sun, A. Colagrossi, S. Marrone, M. Antuono, and A.M. Zhang. A consistent approach to particle shifting in the δ-Plus-SPH model. *Computer Methods in Applied Mechanics and Engineering*, 348:912–934, 2019.

[30] B. Titurus, J. E. Cooper, F. Saltari, F. Mastroddi, and F. Gambioli. Analysis of a sloshing beam experiment. In *International Forum on Aeroelasticity and Structural Dynamics. Savannah, Georgia, USA, paper*, volume 139, 2019.

SPH prediction of energy dissipation in a sloshing tank subjected to vertical harmonic excitations

Salvatore Marrone, Julien Michel
CNR-INM Institute of marine engineering
National Research Council
Rome, Italy,
salvatore.marrone@cnr.it

Francesco Saltari, Franco Mastroddi
Dept. of Mechanical and Aerospace Engineering
Sapienza University of Rome
Rome, Italy

***Abstract*—In [14], [16] the damping effect of sloshing flows on the dynamics of flexible structures was studied through an enhanced SPH model. Prediction of energy dissipation in these problems is of interest, among the others, in the aeronautic field to appropriately address sloshing-induced loads on aircraft wings. In the present work the same SPH scheme is applied and extensively validated on the experimental campaign performed in [25] in which a partially filled tank is subjected to harmonic vertical accelerations ranging from $0.5g$ up to $6g$. Conversely to [14], in the present work long-time simulations are addressed spanning over more than 50 periods of oscillations. This approach allowed us to compare the predicted energy dissipation in terms of average value computed over several tank oscillations. The SPH scheme is tested over a large matrix of different frequencies and accelerations covering a wide range of flow regimes and spanning from mildly-deformed free surface to violent shaken flow. Even if the numerical model is only 2D and air phase is neglected, it is shown that the SPH solver is, in most of the cases, able to recover the experimental rate of dissipated energy with errors comparable to the intrinsic uncertainties of the problem. Considering that no parameter adjustment has been done in any of the performed test cases, this result makes the SPH a valid and competitive numerical solver for the simulation of such complex flows.**

I. Introduction

Sloshing flows are those occurring when free surface waves are generated inside a tank and caused by any disturbance to partially filled containers. Depending on the type of disturbance and container shape, the liquid surface can experience different types of motion including simple planar, rotational, symmetric, asymmetric, quasi-periodic or chaotic. On the other hand, sloshing flows can be effectively used to dampen the oscillations of a structure. Tuned Liquid Dampers (TLD) exploit the liquid sloshing motion in a tank in order to counteract the external forces and dissipate energy. These dampers are of great interest in many engineering fields, spanning from the control of building stability or the rolling motion of ships in the civil engineering, to aerospace where the suppression of spacecraft instabilities is of fundamental importance during the ascent or landing stages [1], [12].

From the physical point of view, the study and prediction of the energy dissipation induced by a free-surface flow is generally arduous, especially in presence of wave breaking. [23] presented a review of studies dedicated to the dissipation caused by wave breaking. From a numerical point of view, several methods have been used to evaluate energy dissipation in breaking waves. As far as SPH modelling of sloshing flows is concerned, in [5] and [6] a dynamical system involving a driven pendulum filled with liquid was studied experimentally and numerically by Smoothed Particle Hydrodynamics (SPH), focusing on the mechanical energy dissipation of the system.

Recently, kerosene containers placed inside aircraft wings have received attention as a complex industrial sloshing problem [9], [11]. During flight, sudden strong gusts accelerate the wing tips up to values of 10g, which results in sloshing amplitudes comparable to the tank dimensions and frequencies higher than 5 Hz (see [10]). This fluid motion, which several experiments have demonstrated to play a role on the damping of the wing vibrations, is significantly different from typical sloshing flows: the fuel is continuously broken into several jets and drops, whilst violently slamming alternately upward and downward against the tank walls.

In [7], [14], [16], such a violent flow has been numerically studied by reproducing the experiments in [17] in which a partially filled tank was subjected to a decaying vertical oscillating motion. The rapidly decaying flow motion on one hand allows one to perform short time simulations but, on the other hand, introduces difficulties in assessing the energy dissipation without solving the full fluid-structure interaction problem (for more details see [14]).

In order to overcome those limitations, in the present work the experiments by [25] are considered. In that experimental campaign a purely harmonic vertical motion is imposed on a partially filled tank. This approach makes possible to evaluate energy dissipation as an average values over multiple oscillation cycles, thus providing a more robust and reliable validation of the adopted SPH solver for this kind of flows, also in terms of convergence analysis. A large test case matrix spanning several motion frequencies and amplitudes has been tested. Further, the relevance of aspects such as surface tension and 3D effects are analysed and discussed, thus extending the findings in [14].